IEEE Access
Multidisciplinary | Rapid Review | Open Access Journal

Received November 4, 2019, accepted November 21, 2019, date of publication November 25, 2019,
date of current version December 11, 2019.

Digital Object Identifier 10.1109/ACCESS.2019.2955805

A Hybrid Compensation Topology With Single Switch for Battery Charging of Inductive Power Transfer Systems

HAILONG ZHANG, (Student Member, IEEE), YAFEI CHEN, (Student Member, IEEE), SUNG-JUN PARK, AND DONG-HEE KIM, (Member, IEEE)
Department of Electrical Engineering, Chonnam National University, Gwangju 61186, South Korea

Corresponding author: Dong-Hee Kim (kimdonghee@jnu.ac.kr)

This work was supported in part by the National Research Foundation of Korea (NRF) grant funded by the Korea Government (MSIT) under Grant NRF-2017R1C1B2010057, and in part by the Korea Institute of Energy Technology Evaluation and Planning (KETEP) and the Ministry of Trade, Industry and Energy (MOTIE) of the Republic of Korea under Grant 20193810100001B.

ABSTRACT This paper presents an inductive-power transfer (IPT) system with load-independent constant current (CC) and constant voltage (CV) charging characteristics for low power systems. An inductor–capacitor–capacitor series (LCC-S) compensation-based hybrid topology that can achieve both CC and CV charging with only one additional switch under zero-phase-angle conditions is proposed. Additionally, the CC/CV charging mode can be realized with two different fixed frequencies. The proposed system has a simple structure and low cost and uses only primary-side electrical information to control the battery charging profile, achieving communication-less control between the primary and secondary sides. It greatly simplifies the controller design process. A 200-W laboratory prototype is built to verify the feasibility of the proposed topology, and the maximum efficiencies of the CC and CV modes are approximately 85% and 87%, respectively.

INDEX TERMS Battery charging, constant-current output, constant-voltage output, inductive power transfer, hybrid compensation topology.

I. INTRODUCTION

Wireless-power-transfer (WPT) systems, which use no connection between the transmitter and the receiver, have the advantages of physical isolation, safety of operation, and reliability, and they ensure normal operation in harsh environments [1]–[3]. These systems have a wide range of applications, such as in EVs (electrical vehicles), drones, mobile phones, and medical implants [4]. Especially in low-power wireless charging applications, such as unmanned aerial vehicles (UAVs) [5], electric bicycles [6], [7], and consumer electronics [8], [9], inductive power transfer (IPT) technology has become a research hotspot by virtue of its inherent advantages.

The output resistance of a battery changes significantly during the entire charging process [10], [11]. Therefore, it is essential to design a stable controller to address parameter changes. The most important method to address this issue is constant current (CC) and constant voltage (CV) charging. The CC/CV charging profile is shown in Fig. 1. As shown in the figure, the battery charging current remains stable in the CC mode and decreases significantly in the CV mode, whereas the battery voltage increases rapidly in the CC mode and is stable in the CV mode. The following methods

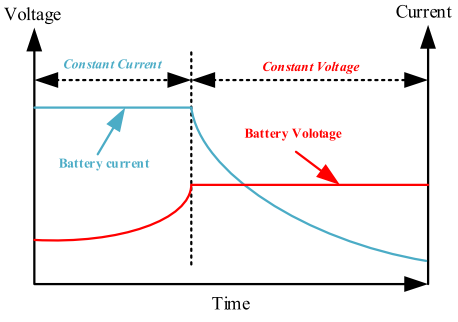

FIGURE 1. Battery charging profile.

The associate editor coordinating the review of this manuscript and approving it for publication was Sze Sing Lee.

This work is licensed under a Creative Commons Attribution 4.0 License. For more information, see http://creativecommons.org/licenses/by/4.0/

can realize CC and CV charging: 1) Using a dc–dc converter on the primary side [10] and secondary side [12]. This method can easily achieve CC and CV charging by controlling the back-end converter. However, it needs additional components and increases the complexity of the system, while it introduces further power loss. 2) Changing the operating frequency. In [13]–[16], a basic topology (SS, SP, PS, PP) can realize CC and CV outputs at two different frequencies. However, this method cannot achieve a constant output and a zero-phase-angle (ZPA) simultaneously. Additionally, this approach suffers from bifurcation and control complexity. In [17], the CC/CV model was realized using two different frequencies in a double side inductor–capacitor–capacitor series (LCC-LCC) topology. The main drawbacks of this technique are an increased number of components and a complex control method. 3) Using hybrid topologies. In [18], hybrid topologies with a load-independent CC or CV output were realized by hybrid topologies with a load-independent CC or CV output were realized by switching the series compensation into parallel compensation on the transmitter side. However, this technique requires the use of three switches and one inductor, it increases the component counts, losses, and complexity. To obtain the ZPA condition during the CC/CV charging process, a hybrid compensation tank with SS and PS or SP and PP was used in [19]; however, additional switches were required to convert the topology. 4) Realization of the CC/CV mode by a control method. To fulfill the CC or CV output requirements under the ZPA condition, [2] introduced a novel method to achieve CC/CV charging with double inductor–capacitor–capacitor (LCC–LCC) topology with two independent operating frequencies. However, this approach is successful only when the self-inductance of the primary coil is equal to that of the secondary one. Phase shift control is another method applied to the full bridge inverter to adjust the CC/CV mode during load variation [20]. However, it is difficult to attain zero voltage switching (ZVS) under a light-load condition. Therefore, all of these methods have limitations.

The common commutation modes between the primary and secondary sides in a WPT system are shown in Fig. 2. Two communication methods are used in a WPT system: wireless communication type, and no communication type. All of the CC/CV charging methods mentioned earlier [1]–[20] require wireless communication (Wi-Fi, Bluetooth, Zigbee) between the primary and secondary sides. Communication may be interrupted owing to cross-technology interference or bad connectivity of the devices [21].

In the communication-less type for WPT system, the output current and voltage are controlled by the primary-side parameters. In [22], the output power was adjusted by the primary side signal acquisition. In [23], the output power was regulated by the frequency droop controller on the primary side. In [24], the CV model was realized for the inductor–capacitor–inductor (LCL) configuration by phase shift control on the primary side. All of these methods are focused

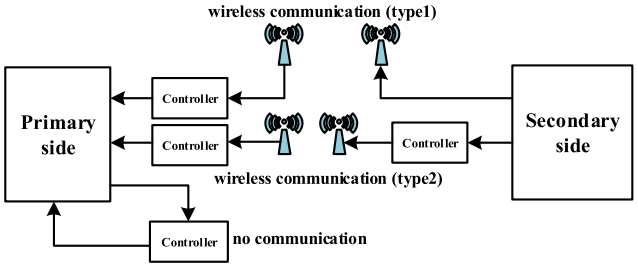

FIGURE 2. Common commutation modes in a WPT system.

on output regulation, and the CC/CV charging process is not analyzed in detail. The quadrature transformation algorithm and a proportional-integral (PI) controlled phase shift controller was proposed in [25] to realize CC/CV mode charging in the inductor–capacitor inductor–series (LCL-S) topology. However, the algorithm was too complicated to realize. Reference [26] proposed a primary-side control method with a weak commutation that can achieve both CC and CV mode charging. Although secondary-side electrical information can be estimated without line communication, the noise interface can be reduced using filters. However, if the mutual inductance information detected in the start-up process is incorrect or the filters break down, the electrical information on the secondary side will not be collected properly.

In light of the above analysis, a topology and control method with the following characteristics is required: 1) No back-end dc–dc converter to control the battery voltage and current. 2) Simple structure of the resonant tank to decrease external power losses. 3) Nearly ZPA condition and soft switching operation during the entire charging process to attain low volt-ampere (VA) rating and low conduction loss of the switches. 4) Fixed resonance frequency in CC and CV charging to avoid bifurcation. In this paper, a novel resonant tank topology and CC/CV control method is proposed to meet the above requirements.

To simplify the controller design of an IPT system and avoid the drawbacks of conventional topologies and control methods, a CC/CV control method based on hybrid compensation topology with single switch is proposed for charging low-power wireless systems. Using detailed analysis of the LCC-S and parallel-series/parallel (PS/S) topology, the CC/CV charging mode can be achieved only by changing the operation frequency and adding an additional switch. This topology can realize ZPA operation with a fixed operating frequency and ZVS, achieving a low VA rating and improving efficiency. Additionally, the battery output voltage and current can be estimated by the acquisition of primary-side electrical information. Therefore, communication-less control can be attained between the primary and secondary sides. The effectiveness of the proposed topology is verified by simulations and an experiment using a 200-W prototype, and the maximum efficiency of the CC and CV modes is approximately 85% and 87%, respectively.

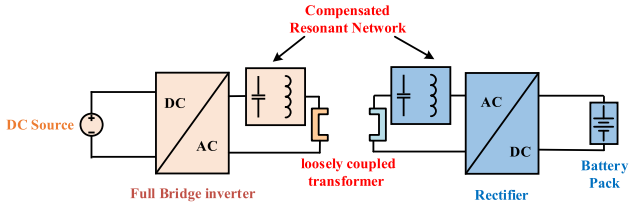

FIGURE 3. Overview of the IPT system.

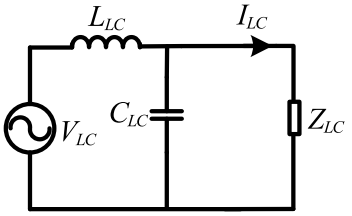

FIGURE 4. LC resonant network.

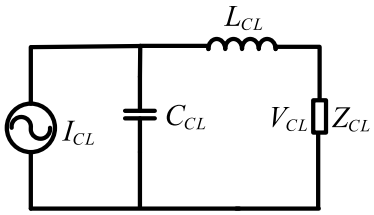

FIGURE 5. CL resonant network.

II. HYBRID TOPOLOGY DESIGN

An overview of the IPT system is shown in Fig. 3. In an IPT system, the basic requirement of the resonant network topology is to minimize the VA rating of the dc source. On the secondary side, the resonant network compensates the inductance of the secondary coil to increase the transfer capability.

Generally, the resonant network consists of two types of component: inductors and capacitors. LC and CL resonant networks are regularly used in IPT systems.

Fig. 4 shows an LC resonant network, where the resonant angular frequency (ω_{LC}) is equal to the angular frequency of the ac voltage source and can be expressed as

$$\omega_{LC} = \frac{1}{\sqrt{L_{LC}C_{LC}}} \tag{1}$$

According to Kirchhoff's law, the output current under the resonance condition is given by

$$\boldsymbol{I}_{LC} = -\boldsymbol{j}V_{LC}\sqrt{\frac{C_{LC}}{L_{LC}}} = -\boldsymbol{j}\frac{\boldsymbol{V}_{LC}}{\omega_{LC}L_{LC}} \tag{2}$$

where $\boldsymbol{V}_{\mathrm{LC}}$ is the input voltage of LC resonant network and $\boldsymbol{I}_{\mathrm{LC}}$ is the value of the output current. Based on (2), when the circuit operates in the resonance condition, the output current of the LC network in constant and independent of Z_{LC}. Therefore, the LC resonant network shows a CC output characteristic.

A CL resonant network is shown in Fig. 5. The resonant angular frequency in a CL resonant tank is the same as that of an LC resonant tank: $\omega_{\mathrm{LC}} = \omega_{\mathrm{CL}}$. The output voltage under

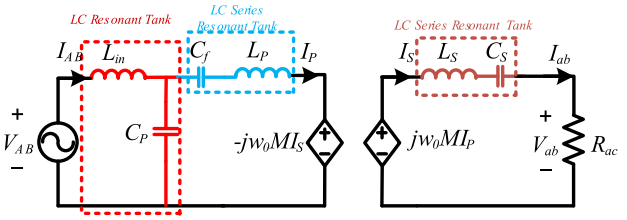

FIGURE 6. M model with LCC-S compensation topology.

the resonance condition can be expressed as

$$\boldsymbol{V}_{CL} = -\boldsymbol{j}\boldsymbol{I}_{CL}\sqrt{\frac{L_{CL}}{C_{CL}}} = -\boldsymbol{j}\omega_{CL}L_{CL}\boldsymbol{I}_{CL} \tag{3}$$

where $\boldsymbol{V}_{\mathrm{CL}}$ is the output voltage of CL resonant network and $\boldsymbol{I}_{\mathrm{CL}}$ is the value of the input current. According to (3), the output voltage of the CL resonant tank is independent of the load variation.

A. REALIZATION OF CV MODE WITH THE ZPA CONDITION

Two well-known models are used in wireless power transfer systems: the M model and the T model. According to [27], the mutual inductance model is appropriate for self-inductance compensation, and the T model is suitable for leakage inductance compensation. In the LCCL-S compensation topology, to satisfy the requirement of the resonance frequency being independent of the coupling coefficient (k), self-inductance compensation is required. In addition, the M model can derive the output characteristics because both sides can be analyzed independently. Consequently, the mutual inductance model meets the requirement of this study.

The M model of the LCC-S compensation topology is shown in Fig. 6. The resonant network has four components. L_{in} and C_p are the series compensation inductor and the parallel compensation capacitor, respectively, on the primary side. C_f and C_s are series compensation capacitors on the primary and secondary sides, respectively. V_{AB} is the input voltage of the resonant network (output of the full bridge inverter) and V_{ab} represents the output voltage of the resonant network (input voltage of the rectifier). I_{AB} and I_{ab} are the input and output currents of the resonant network. R_{ac} is the ac equivalent resistance of the output resistance R_{o}. L_p and L_S are the self-inductance of the primary and secondary coils, respectively, whereas M is the mutual inductance between the transmitter and the receiver; that is, $M = k\sqrt{L_P L_S}$.

From [27], it can be derived that the LC resonant tank has a CC output characteristic under ZPA conditions. The LC series resonant tank can be regarded as one resistance under resonance conditions.

Therefore, according to the duality principle, the LCC-S resonant network shows a load independent constant output voltage characteristic. When L_{in} is resonant with C_p and then L_p, L_{in} is resonant with C_f, it means that the operating frequency is equal to the ZPA frequency, $\omega_{\mathrm{cv}} = 2\pi f_{\mathrm{cv}}$, where f_{cv} is the operating frequency in the CV mode. The angle

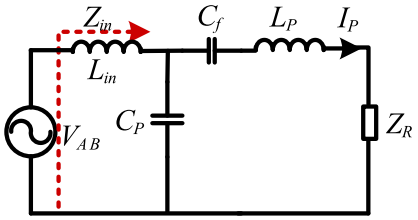

FIGURE 7. Primary circuit with reflected impedance.

frequency can be given by

$$\omega_0 = \omega_{cv} = \frac{1}{\sqrt{L_{in}C_p}} = \frac{1}{\sqrt{L_S C_S}} \tag{4}$$

To simplify the analysis, the model in Fig. 6 can be simplified to be the model shown in Fig. 7. Z_R is the reflection impedance of the secondary side.

According to [28], the impedance of the secondary side Z_S and the reflection impedance Z_R can be derived as

$$\begin{cases} \boldsymbol{Z}_s = j\omega L_S + 1/j\omega C_S + R_{ac} \\ \boldsymbol{Z}_R = \dfrac{(\omega M)^2}{\boldsymbol{Z}_s} \end{cases} \tag{5}$$

The input impedance Z_{in} and phase angle can be expressed as

$$\begin{cases} \boldsymbol{Z}_{in} = \dfrac{1}{1/\left(j\omega L_p + 1/j\omega C_f + \boldsymbol{Z}_R\right) + j\omega C_p} + j\omega L_{in} \\ \theta_{in} = \dfrac{180^\circ}{\pi} tan^{-1} \dfrac{Im(Z_{in})}{Re(Z_{in})} \end{cases} \tag{6}$$

When the operating frequency satisfies equation (4), the input impedance can be calculated as

$$\boldsymbol{Z}_{in} = \frac{\omega_0^2 C_f L_{in} R_{ac}}{(j\omega_0(L_P - L_{in}) + 1/j\omega_0 C_f)R_{ac} + \omega_0^4 M^2 C_P C_f} \tag{7}$$

To satisfy the ZPA condition, the imaginary part of equation (7) is equal to 0, which can be expressed as

$$(j\omega_0(L_P - L_{in}) + 1/j\omega_0 C_f)R_{ac} = 0 \tag{8}$$

To satisfy equation (8), the input inductor L_{in} must be

$$L_{in} = \left(\frac{C_f}{C_f + C_P}\right) L_P \tag{9}$$

It can be concluded that the ZPA condition can be satisfied by selecting the resonance parameter on the primary side to be as shown in Equation (9).

Additionally, the impedance of the primary side can be obtained as

$$Z_{in} = (\frac{L_{in}}{M})^2 R_{ac} \tag{10}$$

The output voltage and the voltage conversion ratio can be derived as

$$\begin{cases} V_{ab} = I_s R_{ac} = \dfrac{MV_{AB}}{L_{in}} \\ G_V = \left|\dfrac{V_{ac}}{V_{AB}}\right| = \dfrac{M}{L_{in}} \end{cases} \tag{11}$$

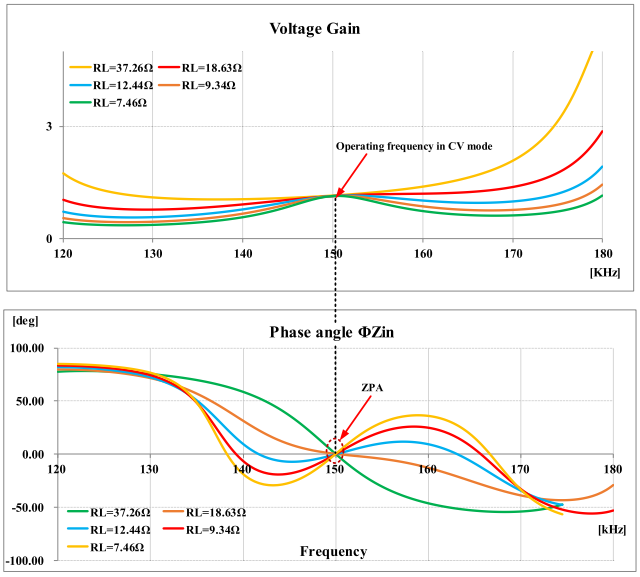

FIGURE 8. Voltage gain and phase of input impedance of the IPT converter.

It can be concluded that the output voltage is load independent at the resonant frequency(150kHz) during the load range (5Ω-60Ω) and that ZPA can be achieved simultaneously. The input current of the resonant network can be expressed as

$$\boldsymbol{I}_{AB} = \frac{V_{AB}}{Z_{in}} = \frac{V_{AB}M^2}{L_{in}^2 R_{ac}} \tag{12}$$

From formulas (11) and (12), it can be seen that the output of the rectifier can be calculated using the current and voltage of the full bridge inverter.

From Fig. 8, the system can be designed in the CV mode to be consistent with the ZPA condition. R_o is the dc load resistance. In this study, R_L is identical with the battery equivalent resistance because the load is the battery ($R_o = R_{Bat}$). According to above analysis, the LCC compensation topology is widely used in WPT systems because it can easily attain ZPA for the input impedance and ZVS for the switches, exhibiting low reactive loss and high system efficiency.

The output current of the LCC-S topology is shown in Fig. 9. In the range of operating frequencies used in this study (140–160 kHz), the output current is highest at the resonance frequency. The ZPA is lost when the operating frequency is far from the resonance point. Additionally, the output current decreases with increasing load resistance, which implies that the output power increases with decreasing load resistance.

B. REALIZATION OF CC MODE WITH THE ZPA CONDITION

By removing the input inductance L_{in} from the LCC-S topology, it becomes the PS/S topology, as shown in Fig. 10. According to the previous analysis, the *LC* series resonant tank can be regarded as one inductor and the *CL* resonant

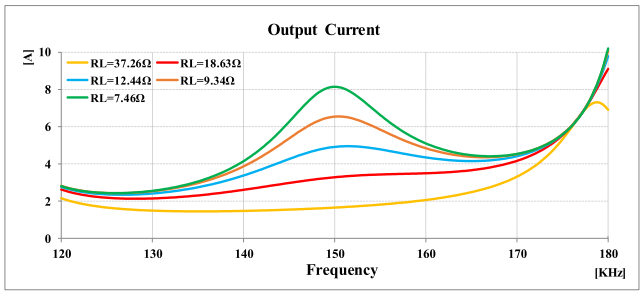

FIGURE 9. Output current of the LCC-S topology.

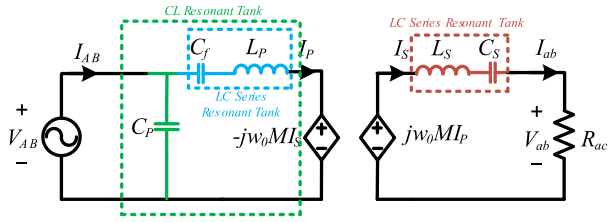

FIGURE 10. Analytical circuit of PS/S compensation topology.

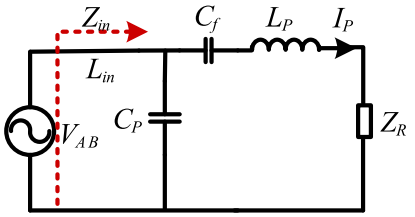

FIGURE 11. Primary circuit with reflected impedance for PS/S topology.

tank has a CV output. According to the duality principle, this implies that PS/S topology has CC output characteristic.

To simplify the calculation according to the model shown in Fig. 11, the input impedance and phase angle can be expressed as

$$\begin{cases} \boldsymbol{Z}_{in} = \dfrac{1}{1/\left(j\omega L_P + 1/j\omega C_f + \boldsymbol{Z}_R\right) + j\omega C_P} \\ \theta_{in} = \dfrac{180^{\circ}}{\pi} tan^{-1} \dfrac{Im(Z_{in})}{Re(Z_{in})} \end{cases} \tag{13}$$

The equivalent impedance and current of the secondary side can be derived as

$$\begin{cases} \boldsymbol{Z}_S = j\omega L_S + \dfrac{1}{j\omega C_S} + R_{ac} \\ I_{ab} = \left| \dfrac{j\omega M V_{AB}}{\boldsymbol{Z}_s \boldsymbol{Z}_{in}\left[1 + j\omega C_P\left(j\omega L_P + 1/j\omega C_f + \boldsymbol{Z}_R\right)\right]} \right| \end{cases} \tag{14}$$

When the resonant network operates in the CC mode, I_{ab} is independent of the output resistance R_{ac}. Assuming that $j\omega L_P + 1/j\omega C_f = \alpha$, the input impedance can be expressed as

$$\boldsymbol{Z}_S = j\omega L_S + \frac{1}{j\omega C_S} + R_{ac} \tag{15}$$

The output current of the resonant network can be given by

$$\boldsymbol{I}_{ab} = \frac{j\omega M V_{AB}}{Z_S(\alpha + (\omega M)^2/Z_S)} \tag{16}$$

When $\alpha = 0$, the real part of I_{ab} can be written as

$$I_{ab} = \frac{V_{AB}}{\omega M} \tag{17}$$

From (17), it can be concluded that the output current is load independent at the resonant frequency(136.5kHz) during the load range (5Ω-60Ω), and the operating frequency is $\omega_{cc} = 2\pi f_{cc}$, where f_{cc} is the operating frequency in the CC mode. The angular frequency is $\omega_0^2 = \omega_{cc}^2 = 1/(L_P C_f)$.

The input resistance can be expressed as

$$\boldsymbol{Z}_{in} = \frac{j(\omega_0 M)^2}{-\omega_0 L_s + 1/\omega_0 C_s - \omega_0^3 M^2 C_P + jR_{ac}} \tag{18}$$

Assuming that $-\omega L_S + 1/\omega C_S - \omega^3 M^2 C_P = \beta$, Z_{in} can be calculated as

$$\boldsymbol{Z}_{in} = \frac{R_{ac}(\omega_0 M)^2 + j\beta(\omega_0 M)^2}{\beta^2 + R_{ac}^2} \tag{19}$$

To ensure that the ZPA condition is satisfied, the angle of the input impedance is maintained at 0. That is, $Im(\mathrm{Z_{in}}) = 0$, which is equivalent to $\beta = 0$.

From [27], it can be concluded that the ZPA can be achieved by tuning the value of C_S, which can be derived as

$$C_S = \frac{1}{\omega_0^4 M^2 C_P + \omega_0^2 L_S} \tag{20}$$

Therefore, ZPA can be easily realized by selecting a suitable value of C_S.

When operating in the CC mode under the ZPA condition, the real part of Z_{in} can be calculated by $Z_{in} = (\omega_0 M)^2/R_{ac}$.

The transconductance gain of the PS/S topology can be expressed by

$$G_T = \frac{I_{ab}}{V_{AB}} = \frac{1}{\omega_0 M} \tag{21}$$

It can be derived that the CC output is independent of the output resistance.

The output current of the full bridge inverter can be given by

$$I_{AB} = \frac{V_{AB} R_{ac}}{(\omega_0 M)^2} \tag{22}$$

The output voltage of the rectifier can be expressed as

$$V_{ab} = \frac{V_{AB} R_{ac}}{\omega_0 M} \tag{23}$$

From formulas (22) and (23), the output current and voltage of the rectifier can be calculated according to the input characteristics of the full bridge inverter.

As shown in Fig. 12, the PS/S compensation topology can easily achieve ZPA and ZVS simultaneously. Additionally, the output current is load-independent. Further, the operating frequencies in the CC and CV modes are different. The operating frequency in the CC mode is lower than that of the CV mode; therefore, the switching loss in the CC mode is lower than that in the CV mode.

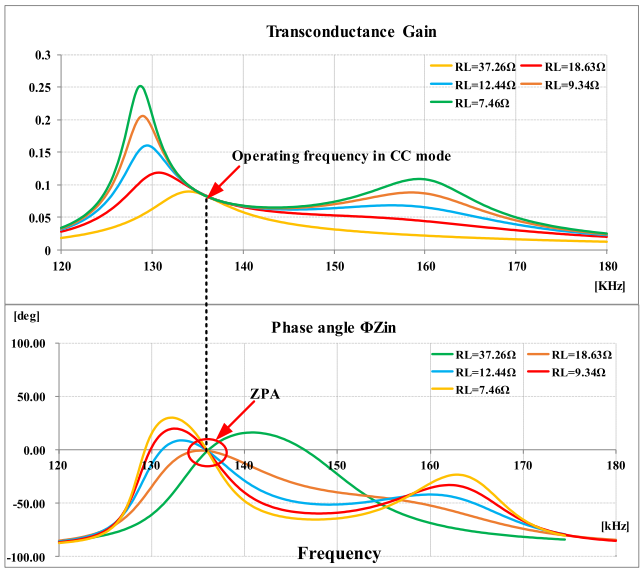

FIGURE 12. Transconductance gain and phase of the input impedance in the PS/S topology.

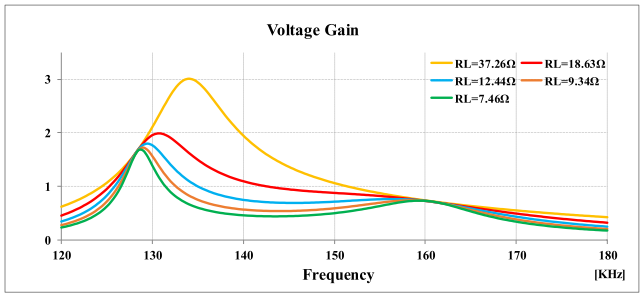

FIGURE 13. Voltage gain of the PS/S topology.

TABLE 1. Design parameters of the resonant network.

Parameter	Value
L_P	62.03 μH
L_S	62.34 μH
L_{in}	11.16 μH
C_P	102 nF
C_f	22.1 nF
C_S	18.4 nF
f_{cc}	150 kHz
f_{cv}	136.5 kHz
M	12.43 μH
k	0.20

When operating in the CC mode under the ZPA condition, the real part of Z_{in} can be calculated as $Z_{\text{in}} = (\omega M)^2/R_{ac}$.

The voltage gain curve of the PS/S topology is shown in Fig. 13. It can be concluded that the voltage gain ratio decreases with increasing operating frequency (133–143 kHz). The voltage conversion ratio and output power increase with decreasing load resistance.

The *Cs* value of the CC mode is calculated to be approximately equal to that of the CV mode. Therefore, to simplify the implementation of the controller and reduce cost, a unified resonance network is selected for the CC and CV modes, and the parameters are shown in Table 1.

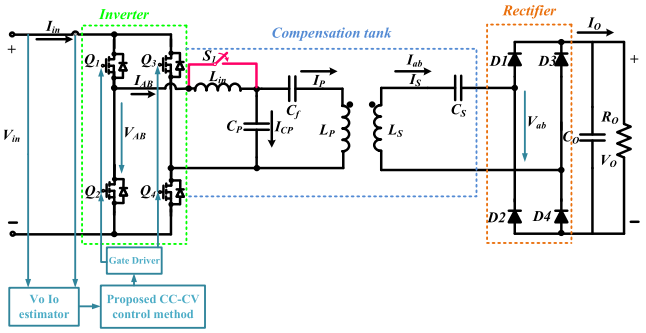

FIGURE 14. System structure and control diagram.

III. PROPOSED CC–CV CONTROL METHOD

The overall system structure and control diagram are shown in Fig. 14. Q_1–Q_4 are four MOSFETs on the side of the full bridge inverter; D_1–D_4 are rectifier diodes; V_{in} is the dc input voltage; V_{o} and I_{o} represent the output voltage and current, respectively; and R_{o} is the output resistance. A low-cost relay is used as a switch to change the charging mode, because the switching time does not affect the performance of the battery charging system [29]. The midpoint voltage of the full bridge inverter U_{AB} is expanded in a Fourier series, and U_{AB} can be given by

$$V_{AB} = \frac{4V_{in}}{\pi} \sum_{n=1,3,5\cdots} \frac{sin(n\varphi)}{n} \tag{24}$$

where n is the number of harmonics, and φ is the phase angle. The quality factors of the compensation networks in a WPT system are relatively high. Thus, fundamental harmonic analysis can be utilized in the proposed system. In this case, because only the fundamental component is considered, $n = 1$. According to [29], the inputs of the dc source and of the resonant network (rms value) components have the following relationship

$$\begin{cases} V_{AB} = \dfrac{2\sqrt{2}V_{in}}{\pi} \\ I_{AB} = \dfrac{2\sqrt{2}I_{in}}{\pi} \end{cases} \tag{25}$$

The relationship of the input of the rectifier (rms value) and the output of battery bank can be given as [31]

$$\begin{cases} V_O = \dfrac{2\sqrt{2}V_{ab}}{\pi} \\ I_O = \dfrac{\pi I_{ab}}{2\sqrt{2}} \end{cases} \tag{26}$$

Therefore, the DC/AC and AC/DC relationship in terms of input side and output side of the overall system can be obtained from (25) and (26). The ac equivalent resistance can be derived by the equation $R_{\text{ac}} = 8R_{\text{o}}/\pi^2$, where the ac voltage and current are rms values.

In previous studies, the primary and secondary sides of the WPT system required wireless communications, such as Bluetooth, Wi-Fi, and ZigBee, which demand high transmission accuracy. Additionally, the cost of the system and

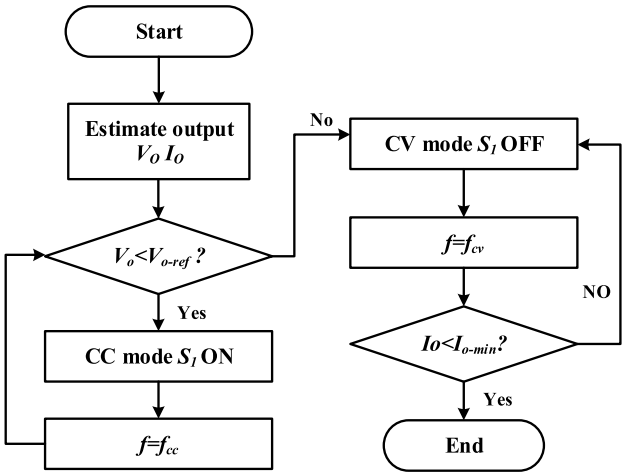

FIGURE 15. Flowchart of the proposed CC/CV control method.

the complexity of the controller also increased. The control method proposed here estimates the output electrical information by sampling the dc input voltage and current and then changes the operating frequency according to the value of the output voltage. When the output voltage is lower than the battery reference voltage, the controller operates in the CC mode. In this mode, switch S_1 is on and the operating frequency is equal to f_{cc}. When the output voltage is equal to or greater than the battery reference voltage, the controller operates in the CV mode. At this time, switch S_1 is off and the operating frequency is equal to f_{cv}. The charging process is finished when the output current reaches its minimum value. Therefore, without the need of control signals on the secondary side, the CC/CV output can be realized only by controlling the frequency of the primary side and the switching state of S_1.

In the CC mode, the battery output voltage can be derived by combining the equations (23), (25) and (26), and the output current in the CV mode can be calculated by (12), (25) and (26). Therefore, the output voltage and current can be estimated by the input DC value. A flowchart of the control method is shown in Fig. 15. It can be concluded that the proposed controller is simple in terms of structure and easy to operate. According to the control method, the battery reference voltage is 52 V and the minimum battery current is set to 0.9A.

IV. SIMULATION AND EXPERIMENTAL RESULTS

To verify the proposed topology and control method, a 200-W prototype was built. The characteristic parameters of the prototype are listed in Table 2.

Fig. 16(a) shows the converters used in the wireless power transfer system. DSP28335 is used as the main controller. Switches Q_1–Q_4 (IPB031N08N5) are used in the full bridge inverter, and diodes D_1–D_4 (DSA30I100PA) are employed for the rectifier. Chroma 63200A is used as the electronic load to simulate the change of the battery equivalent load. Fig. 16(b) shows the primary side and secondary side coils,

TABLE 2. Parameters of the proposed topology.

Parameter	Symbol	Value
Input voltage	V_{in}	48 V dc
Output voltage	V_o	52 V dc
Output power	P_o	200 W
Switching frequency	f_{cc}	137 kHz
Switching frequency	f_{cv}	149 kHz

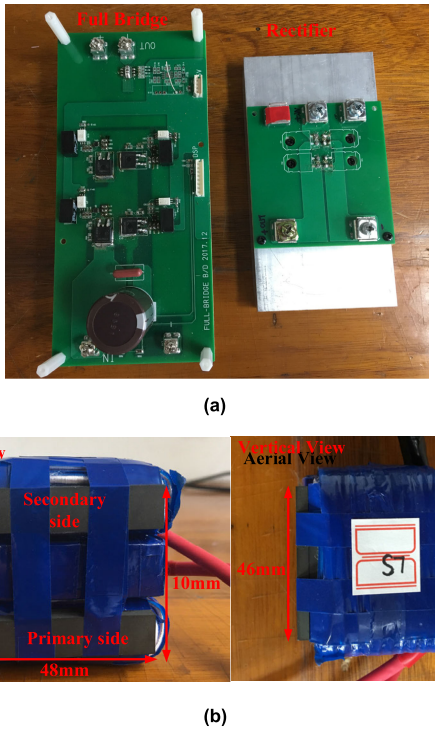

FIGURE 16. Prototype of the proposed topology (a) Full bridge inverter and rectifier. (b) Primary and secondary coils.

which are separated by an air gap of 1.5 cm. Litz wire AWG 13 is selected for L_P, L_S, and L_{in} to eliminate skin and proximity effects. The magnetic material of both primary and secondary coils is PM11 ferrite. A C-C type core is selected for the experiment.

To decrease the influence of the reactive power, the operating frequency usually deviates slightly from the resonance point to realize soft switching with reasonable reactive power. This has the obvious advantages of the operating frequency being constant and independent of the load variation during the CC/CV charging mode. Consequently, the proposed design method is simple in structure and easily ensures the stability of the WPT system.

Fig. 17(a) shows the experimental results of the battery output waveforms and the full bridge inverter output waveforms in the CV mode. The output voltage is 52 V and the maximum output power is 200 W. The operating frequency is 149 kHz in the CV mode for soft switching. Fig. 17(b) is the output waveform obtained under load variation. It can be seen that when the output resistance decreases from 13 Ω to 24 Ω, the output power decreases from 200 W to 110 W and the output current decreases from 3.8 A to 2.2 A. The battery

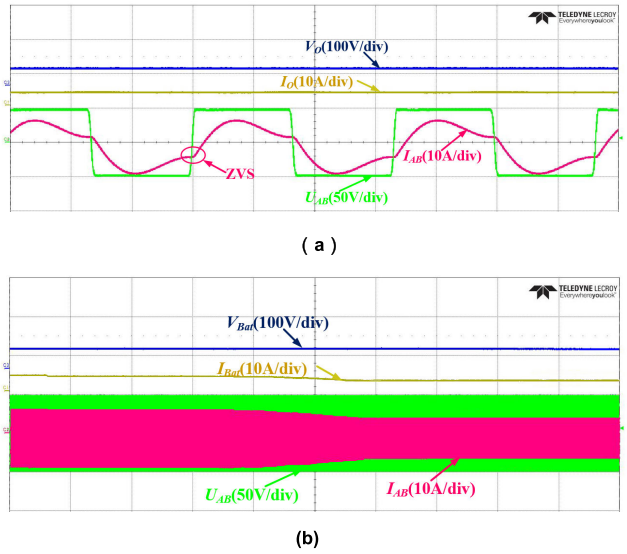

FIGURE 17. Experimental waveforms of V_o, I_o, V_{AB}, and I_{AB} in the CV mode (a) with fixed R_o. (b) with R_o varying from 13 Ω to 24 Ω.

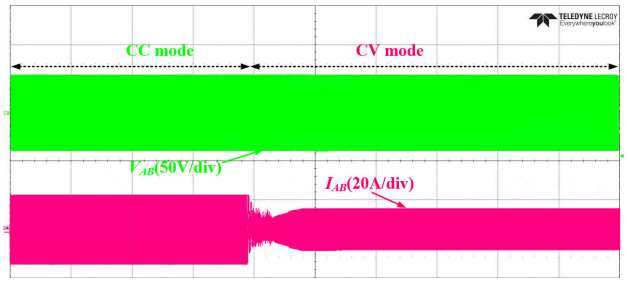

FIGURE 18. Transient waveforms from CC mode to CV mode of proposed topology.

output voltage is stable at 52 V even under varying load conditions. As a consequence, the output voltage remains constant to meet the design requirements.

The transient waveforms of the charging mode from CC to CV are given in Fig. 18. There are some oscillations during the transient switching mode, and it takes around 2 ms to return to the steady state. The output V_{AB} and I_{AB} nearly remains stable after mode switching.

Fig. 19 (a)show the output characteristics of the full bridge inverter and the rectifier under the CC condition. The output power is identical with that of the CV mode. From Fig.17(a) and 19(a), it can be concluded that the inverter can achieve ZVS in CC and CV mode, which agrees well with the theoretical analysis. Fig. 19(b) shows the output waveforms under load variation. It can be seen that when the output resistance increases from 10 Ω to 13 Ω, the output power increases from 110 W to 200 W, the output voltage increases from 38 V to 51 V, and the output current remains constant to meet design requirements.

The output characteristics of the CC/CV mode with multi-load variation are shown in Fig. 20. Fig. 20(a) shows the waveforms in the CV mode, where the output current increases from 2.2 A to 3.8 A and then decreases to 0.9 A and the output resistance varies between 13 Ω to 58 Ω.

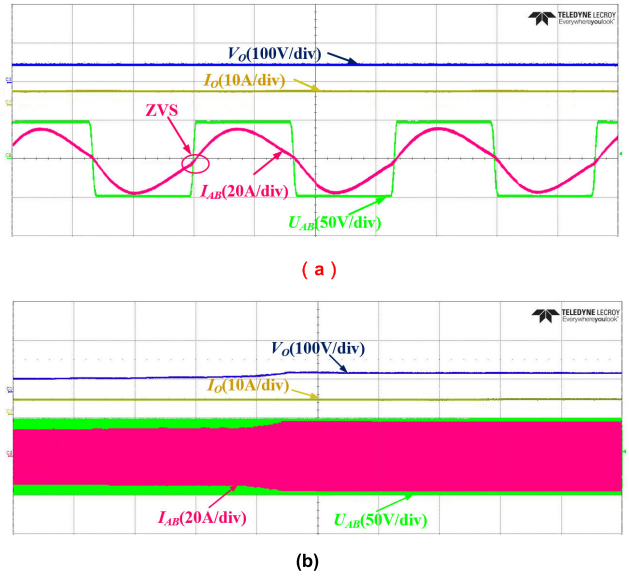

FIGURE 19. Experimental waveforms of V_o, I_o, V_{AB}, and I_{AB} in the CC mode (a) with fixed R_o. (b) with R_o varying from 10 Ω to 13 Ω.

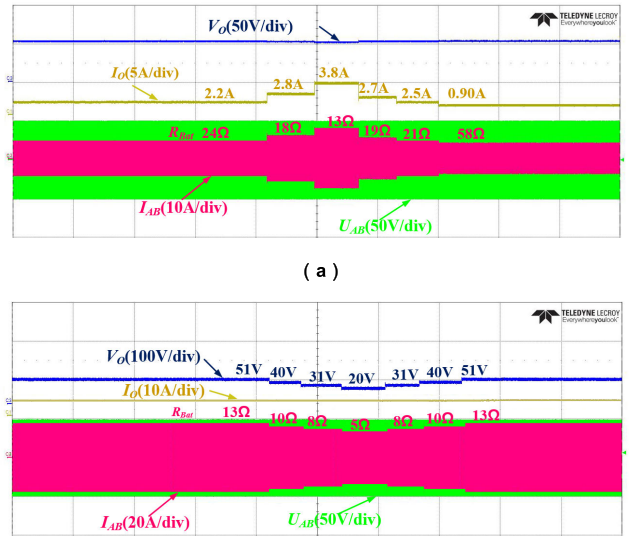

FIGURE 20. Experimental waveforms of V_o, I_o, V_{AB}, and I_{AB} with multi-load regulation (a) CC mode. (b) CV mode.

The output voltage is stable at 52 V, confirming that the results are consistent with the CV mode requirements. When operating in the CC mode, as shown in Fig. 20(b), the output voltage decreases from 51 V to 20 V and then increases to 51 V and the output resistance vary between 5.3 Ω and 13 Ω. The results demonstrate that the battery current is stable at 3.8 A, and the results are consistent with the CC mode requirements.

Fig. 21 shows the overall battery charging profile. The charging voltage increases from 20 V to 52 V, and the charging current range is 0.9 A–3.8 A. Fig. 22 shows the overall system efficiency and output power during the entire charging process. It can be concluded that the average efficiency of the CC mode is higher than that of the CV mode. The maximum

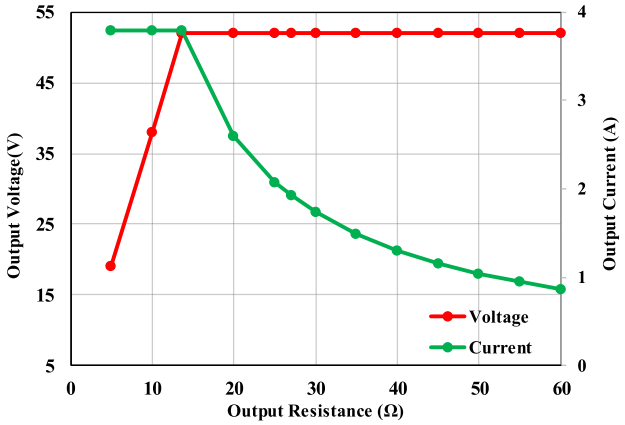

FIGURE 21. Battery voltage and profiles with resistance variations.

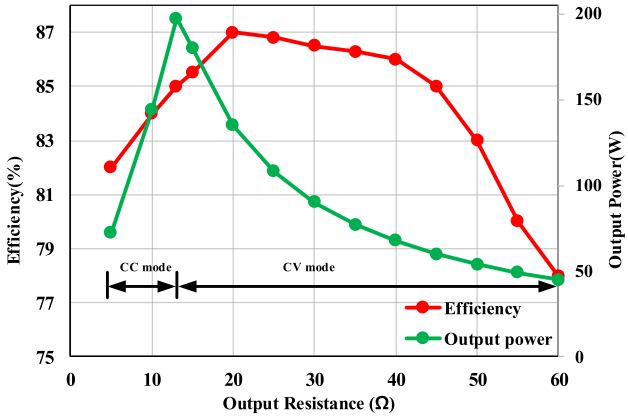

FIGURE 22. Overall system efficiency and output power under the CC/CV charging modes.

efficiency of the overall system is 87%. The maximum output power is obtained at the boundary of the CC/CV modes, and the output power varies from 46 W to 200 W.

V. CONCLUSION

This paper proposes a hybrid compensation topology and a CC/CV control method for low-inductive-power transfer systems. To facilitate the analysis, an M model of the LCC-S and PS/S topologies is built and analyzed in detail. Based on the analysis, the CV and CC modes can be realized by using one hybrid topology at two fixed frequencies. Compared with other similar topologies, the proposed topology has smaller components and volume because of the use of only one additional ac switch. Additionally, the proposed control method can achieve CC/CV charging only by the primary controller. The wireless communication problem can be neglected. The proposed topology and control method are verified by simulation and experimental results using a 200- W prototype, and the measured efficiencies, 85% and 87%, in the CC and CV modes, respectively. The results demonstrate that the proposed topology and control method are suitable for low-power wireless charging systems.

REFERENCES

[1] S. Li and C. C. Mi, "Wireless power transfer for electric vehicle applications," *IEEE J. Emerg. Sel. Topics Power Electron.*, vol. 3, no. 1, pp. 4–17, Mar. 2015.

[2] G. A. Covic and J. T. Boys, "Modern trends in inductive power transfer for transportation applications," *IEEE J. Emerg. Sel. Topics Power Electron.*, vol. 1, no. 1, pp. 28–41, Mar. 2013.

[3] X. Lu, D. Niyato, P. Wang, D. I. Kim, and Z. Han, "Wireless charger networking for mobile devices: Fundamentals, standards, and applications," *IEEE Wireless Commun.*, vol. 22, no. 2, pp. 126–135, Apr. 2015.

[4] C.-S. Wang, G. A. Covic, and O. H. Stielau, "Investigating an LCL load resonant inverter for inductive power transfer applications," *IEEE Trans. Power Electron.*, vol. 19, no. 4, pp. 995–1002, Jul. 2004.

[5] J. M. Arteaga, S. Aldhaher, G. Kkelis, D. C. Yates, and P. D. Mitcheson, "Multi-MHz IPT systems for variable coupling," *IEEE Trans. Power Electron.*, vol. 33, no. 9, pp. 7744–7758, Sep. 2018.

[6] R. Mai, Y. Chen, Y. Zhang, N. Yang, G. Cao, and Z. He, "Optimization of the passive components for an S-LCC topology-based WPT system for charging massive electric bicycles," *IEEE Trans. Ind. Electron.*, vol. 65, no. 7, pp. 5497–5508, Jul. 2018.

[7] H. Z. Z. Beh, G. A. Covic, and J. T. Boys, "Investigation of magnetic couplers in bicycle kickstands for wireless charging of electric bicycles," *IEEE J. Emerg. Sel. Topics Power Electron.*, vol. 3, no. 1, pp. 87–100, Mar. 2015.

[8] S. Y. Hui, "Planar wireless charging technology for portable electronic products and Qi," *Proc. IEEE*, vol. 101, no. 6, pp. 1290–1301, Jun. 2013.

[9] Y. Jang and M. M. Jovanovic, "A contactless electrical energy transmission system for portable-telephone battery chargers," *IEEE Trans. Ind. Electron.*, vol. 50, no. 3, pp. 520–527, Jun. 2003.

[10] H. H. Wu, A. Gilchrist, K. D. Sealy, and D. Bronson, "A high efficiency 5 kW inductive charger for EVs using dual side control," *IEEE Trans. Ind. Informat.*, vol. 8, no. 3, pp. 585–595, Aug. 2012.

[11] W. Zhang, S.-C. Wong, C. K. Tse, and Q. Chen, "An optimized track length in roadway inductive power transfer systems," *IEEE J. Emerg. Sel. Topics Power Electron.*, vol. 2, no. 3, pp. 598–608, Sep. 2014.

[12] Y.-L. Li, Y. Sun, and X. Dai, "μ-synthesis for frequency uncertainty of the ICPT system," *IEEE Trans. Ind. Electron.*, vol. 60, no. 1, pp. 291–300, Jan. 2013.

[13] Z. Huang, S.-C. Wong, and C. K. Tse, "Design methodology of a series-series inductive power transfer system for electric vehicle battery charger application," in *Proc. IEEE Energy Convers. Congr. Expo.*, Sep. 2014, pp. 1778–1782.

[14] W. Zhang, S.-C. Wong, C. K. Tse, and Q. Chen, "Design for efficiency optimization and voltage controllability of series-series compensated inductive power transfer systems," *IEEE Trans. Power Electron.*, vol. 29, no. 1, pp. 191–200, Jan. 2014.

[15] W. Zhang, S.-C. Wong, C. K. Tse, and Q. Chen, "Load-independent current output of inductive power transfer converters with optimized efficiency," in *Proc. Int. Power Electron. Conf.*, May 2014, pp. 1425–1429.

[16] X. Qu, S.-C. Wong, C. K. Tse, and G. Zhang, "Design consideration of a current-source-output inductive power transfer LED lighting system," in *Proc. IEEE Energy Convers. Congr. Expo.*, Sep. 2014, pp. 3607–3611.

[17] V.-B. Vu, D.-H. Tran, and W. Choi, "Implementation of the constant current and constant voltage charge of inductive power transfer systems with the double-sided LCC compensation topology for electric vehicle battery charge applications," *IEEE Trans. Power Electron.*, vol. 33, no. 9, pp. 7398–7410, Sep. 2018.

[18] X. Qu, H. Han, S.-C. Wong, C. K. Tse, and W. Chen, "Hybrid IPT topologies with constant current or constant voltage output for battery charging applications," *IEEE Trans. Power Electron.*, vol. 30, no. 11, pp. 6329–6337, Nov. 2015.

[19] R. Mai, Y. Chen, Y. Li, Y. Zhang, G. Cao, and Z. He, "Inductive power transfer for massive electric bicycles charging based on hybrid topology switching with a single inverter," *IEEE Trans. Power Electron.*, vol. 32, no. 8, pp. 5897–5906, Aug. 2017.

[20] A. Berger, M. Agostinelli, S. Vesti, J. A. Oliver, J. A. Cobos, and M. Huemer, "A wireless charging system applying phase-shift and amplitude control to maximize efficiency and extractable power," *IEEE Trans. Power Electron.*, vol. 30, no. 11, pp. 6338–6348, Nov. 2015.

[21] Z. Zhao, W. Dong, G. Chen, G. Min, T. Gu, and J. Bu, "Embracing corruption burstiness: Fast error recovery for ZigBee under Wi-Fi interference," *IEEE Trans. Mobile Comput.*, vol. 16, no. 9, pp. 2518–2530, Sep. 2017.

[22] J. P.-W. Chow, H. S.-H. Chung, and C.-S. Cheng, "Use of transmitter-side electrical information to estimate mutual inductance and regulate receiver-side power in wireless inductive link," *IEEE Trans. Power Electron.*, vol. 31, no. 9, pp. 6079–6091, Sep. 2016.
[23] U. K. Madawala, M. Neath, and D. J. Thrimawithana, "A power–frequency controller for bidirectional inductive power transfer systems," *IEEE Trans. Ind. Electron.*, vol. 60, no. 1, pp. 310–317, Jan. 2013.
[24] K. Song, Z. Li, J. Jiang, and C. Zhu, "Constant current/voltage charging operation for series-series and series-parallel compensated wireless power transfer systems employing primary-side controller," *IEEE Trans. Power Electron.*, vol. 33, no. 9, pp. 8065–8080, Sep. 2018.
[25] Z. Li, G. Wei, S. Dong, K. Song, and C. B. Zhu, "Constant current/voltage charging for the inductor–capacitor–inductor-series compensated wireless power transfer systems using primary-side electrical information," *IET Power Electron.*, vol. 11, no. 14, pp. 2302–2310, Nov. 2018.
[26] F. Liu, K. Chen, Z. Zhao, K. Li, and L. Yuan, "Transmitter-side control of both the CC and CV modes for the wireless EV charging system with the weak communication," *IEEE J. Emerg. Sel. Topics Power Electron.*, vol. 6, no. 2, pp. 4401–4409, Oct. 2017.
[27] Y. Wang, Y. Yao, X. Liu, D. Xu, and L. Cai, "An LC/S compensation topology and coil design technique for wireless power transfer," *IEEE Trans. Power Electron.*, vol. 33, no. 3, pp. 2007–2025, Mar. 2018.
[28] M. Kim, D.-M. Joo, and B. K. Lee, "Design and control of inductive power transfer system for electric vehicles considering wide variation of output voltage and coupling coefficient," *IEEE Trans. Power Electron.*, vol. 34, no. 2, pp. 1197–1208, Feb. 2019.
[29] R. L. Steigerwald, "A comparison of half-bridge resonant converter topologies," in *Proc. IEEE Appl. Power Electron. Conf. Expo.*, Oct. 1987, pp. 135–144.
[30] C. Auvigne, P. Germano, D. Ladas, and Y. Perriard, "A dual-topology ICPT applied to an electric vehicle battery charger," in *Proc. Int. Conf. Elect. Mach.*, Sep. 2012, pp. 2287–2292.
[31] Y. Chen, H. Zhang, S.-J. Park, and D.-H. Kim, "A switching hybrid LCC-S compensation topology for constant current/voltage EV wireless charging," *IEEE Access*, vol. 7, pp. 133924–133935, Sep. 2019.

HAILONG ZHANG (S'18) received the B.S. degree in electronic engineering and automation from China Petroleum University, Dongying, China, in 2013, and the M.S. degree in control theory and control engineering from the Qingdao University of Science and Technology, Qingdao, China, in 2016. He is currently pursuing the Ph.D. degree in electrical engineering with Chonnam National University, Gwangju, South Korea. His research interests include wireless power transfer system for UAVs, power conversion systems for EVs, and renewable energy storage systems.

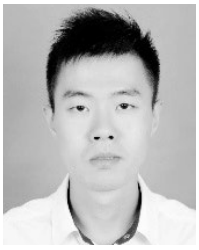

YAFEI CHEN (S'18) received the B.S. degree in electronic information engineering from Southwest Jiaotong University, Chengdu, China, in 2012, and the M.S. degree in control theory and control engineering from the Qingdao University of Science and Technology, Qingdao, China, in 2016. He is currently pursuing the Ph.D. degree in electrical engineering with Chonnam National University, Gwangju, South Korea. His research interests include power conditioning system dc–dc converters for renewable energy, battery chargers for hybrid electric vehicles (HEVs)/EVs, and wireless power transfer for EVs and unmanned aerial vehicles (UAVs).

SUNG-JUN PARK received the B.S., M.S., and Ph.D. degrees in electrical engineering and the Ph.D. degree in mechanical engineering from Pusan National University, Busan, South Korea, in 1991, 1993, 1996, and 2002, respectively. From 1996 to 2000, he was an Assistant Professor with the Department of Electrical Engineering, Koje College, Geoje, South Korea. From 2000 to 2003, he was an Assistant Professor with the Department of Electrical Engineering, Tongmyong College, Busan. Since 2003, he has been a Professor with the Department of Electrical Engineering, Chonnam National University, Gwangju, South Korea. His research interests include power electronics, motor control, mechatronics, and micromachine automation.

DONG-HEE KIM (S'10–M'15) received the B.S., M.S., and Ph.D. degrees from Sungkyunkwan University, Suwon, South Korea, in 2009, 2011, and 2015, respectively, all in electrical engineering.

From 2015 to 2016, he was a Postdoctoral Researcher with Sunkyunkwan University. Since 2016, he has been a part-time Lecturer with Daejin University, Pocheon, South Korea, and the Shandong University of Technology, Shandong, China. From September 2016 to August 2017, he was an Assistant Professor with Tongmyong University, Busan, South Korea. In September 2017, he joined Chonnam National University, Gwangju, South Korea, as an Assistant Professor. His research interests include power conditioning system dc–dc converters for renewable energy, battery chargers for hybrid electric vehicles/electric vehicles, and wireless power transfer for EVs and UAVs.